Protein arginine phosphorylation and de-phosphorylation facilitate protein homeostasis by an AAA+ chaperone protease system

Regina Alver[1,2,4], Ingo Hantke[2,4], Fabián A. Cornejo[1], Katrin Gunka[2], Sebastian Rämisch[1], Noël Molière[2], Emmanuelle Charpentier[1,3] & Kürşad Turgay[1,2*]

[1]*Max Planck Unit for the Science of Pathogens, Berlin, Germany*
[2]*Institut für Mikrobiologie, Leibniz-Universität Hannover, Hannover, Germany*
[3]*Institut für Biologie, Humboldt-Universität zu Berlin, Berlin, Germany*

[4]The authors contributed equally to this work.

[*]for correspondence: Kürşad Turgay, Max Planck Unit for the Science of Pathogens, Charitéplatz 1, 10117 Berlin, Germany; e-mail turgay@mpusp.mpg.de

Running title: protein arginine phosphorylation in protein homeostasis

Keywords: Stress response, protein arginine phosphorylation, protein homeostasis, chaperones, AAA+ proteins, adaptor proteins, McsB kinase, YwlE phosphatase, ClpCP

Abstract

In the Gram-positive model organism *Bacillus subtilis*, the AAA+ unfoldase ClpC associated with the ClpP protease plays an important role in cellular protein homeostasis and stress response. Here, we could demonstrate that the protein arginine kinase and adaptor protein McsB, its activator McsA, the phosphatase YwlE, and ClpC form a unique chaperone system necessary for protein aggregate removal *in vivo* and *in vitro*. Activated McsB phosphorylates and targets aggregated substrate proteins for extraction and unfolding by ClpC. Sub-stoichiometric amounts of catalytically active YwlE significantly enhanced ClpC/McsB-mediated disaggregation and facilitated the refolding of unfolded, arginine-phosphorylated substrate proteins *in vitro*. The refolded substrate proteins could escape the degradation by the associated ClpP protease. In this unique chaperone system, protein unfolding, coordinated with protein arginine phosphorylation and de-phosphorylation, facilitates protein refolding and homeostasis.

Introduction

Molecular chaperone systems monitor and maintain cellular protein homeostasis. These include the highly conserved Hsp60 (GroE) and the Hsp70 (DnaKJE) systems which can prevent aggregation or refold and repair misfolded proteins. In many bacteria and yeast, AAA+ unfoldases such as Hsp104 (ClpB), can disaggregate and refold protein aggregates together with DnaK. In addition, related AAA+ protease complexes, such as ClpCP of *B. subtilis*, allow the general proteolysis and removal of potentially toxic, damaged proteins, which otherwise cannot be rescued or repaired. The substrate recognition and selection by these AAA+ unfoldases often depends on their interaction with adaptor proteins that can recognize and target substrate proteins and thereby define and expand the substrate spectrum. Notably, the control of adaptor protein activity and substrate recognition allows such AAA+ protease complexes to be involved in regulatory proteolysis, controlling, for example, the activity and stability of key transcription factors of stress response or developmental pathways (Battesti and Gottesman, 2013; Hartl et al., 2011; Kirstein et al., 2009; Mogk et al., 2011, 2018; Sauer and Baker, 2011). In these molecular machines, the substrate proteins are recognized and subsequently unfolded by ATPase-driven translocation through the central pore formed by the hexameric AAA+ proteins. The emerging unfolded polypeptide chain can be transferred for degradation into an associated compartmentalized ClpP protease complex (Mogk et al., 2018; Sauer and Baker, 2011; Weibezahn et al., 2004). The association of AAA+ proteins with ClpP is mediated by the tips of ClpP-interacting loops (P-loops) extending from the bottom of the AAA+ protein hexamer and interacting with binding pockets on the apical surface of the double-heptameric ClpP complex (Amor et al., 2019; Fei et al., 2020; Gatsogiannis et al., 2019; Kim et al., 2001; Ripstein et al., 2020; Weibezahn et al., 2004).

In *B. subtilis*, all the highly conserved chaperone systems are present, with the notable exception of the ClpB disaggregase. In addition to their role in general proteolysis, the *B. subtilis* AAA+ protease complexes ClpCP and ClpXP together with their different adaptor proteins are

54 intricately involved in regulatory proteolysis to control e.g. heat and oxidative stress response
55 or cell developmental pathways, such as competence development (Gerth et al., 2004; Hantke
56 et al., 2019; Kirstein et al., 2009; Krüger et al., 1994; Msadek et al., 1994; Runde et al., 2014;
57 Turgay et al., 1998). For *B. subtilis* ClpC, substrate recognition and its activation depend on its
58 three known adaptor proteins, MecA (Turgay et al., 1998), its paralog YpbH (Persuh et al.,
59 2002; Schlothauer et al., 2003) and the protein kinase McsB. The gene for McsB is part of the
60 *clpC* operon (*ctsR*, *mcsA*, *mcsB* and *clpC*) that is, like *clpP* and *clpE* genes, controlled by the
61 heat-sensitive transcription repressor CtsR (Derre et al., 1999; Elsholz et al., 2010, 2011;
62 Fuhrmann et al., 2009; Kirstein et al., 2007, 2009; Krüger and Hecker, 1998; Krüger et al.,
63 2000, 2001).
64 The protein kinase activity of the McsB adaptor protein catalyzes the formation of a phospho-
65 arginine protein modification with a high-energy phosphoramidate bond (Fuhrmann et al.,
66 2009). McsB autophosphorylates itself and McsA, further activating the McsB arginine kinase
67 activity, resulting in enhanced autophosphorylation and the phosphorylation of McsA, ClpC
68 and substrate proteins such as CtsR. YwlE is the cognate phospho-arginine phosphatase, which
69 can counteract the McsB kinase activity, thereby controlling the extent of this protein
70 modification in *B. subtilis* (Elsholz et al., 2012; Fuhrmann et al., 2009, 2013; Kirstein et al.,
71 2005, 2007; Schmidt et al., 2014; Suskiewicz et al., 2019; Trentini et al., 2016). The pleiotropic
72 influence of *ywlE* on *B. subtilis* physiology and regulatory pathways was observed (Elsholz et
73 al., 2012; Schmidt et al., 2014), more recently an important role of YwlE in *B. subtilis* spore
74 germination was discovered (Zhou et al., 2019, 2022).
75 McsB, as an adaptor protein, can interact with the NTD of ClpC and thereby targets the substrate
76 protein for ClpCP degradation. This activity can also occur independently of arginine
77 phosphorylation of the substrate (Elsholz et al., 2010; Kirstein et al., 2007; Stannek et al., 2014).
78 A clear link between the kinase activity of McsB, ClpC activation and its ability to target
79 substrate proteins was observed (Elsholz et al., 2012; Kirstein et al., 2005, 2007; Trentini et al.,

80 2016). Recently, another mechanism of substrate targeting to ClpC could be observed, where
81 protein arginine phosphorylation by McsB could create a degron to mark a model substrate
82 protein for direct recognition by the N-terminal domain of ClpC and subsequent degradation
83 by ClpCP (Morreale et al., 2022; Trentini et al., 2016).
84 The genetic organization and the stress-controlled expression of McsB, McsA and ClpC could
85 indicate a possible role of McsB, McsA and ClpC not only in the control of CtsR but also in
86 general protein homeostasis during stress response. McsB co-localizes with stress-induced sub-
87 cellular protein aggregates (Kirstein et al., 2008) and is necessary for disassembling large
88 proteinaceous structures, such as the DNA uptake complex during the escape from competence
89 (Hahn et al., 2009).
90 Here, we can demonstrate that the McsB kinase is the major ClpC adaptor protein necessary to
91 remove protein aggregates. ClpC, McsB and McsA, in the presence of sub-stoichiometric
92 amounts of YwlE phosphatase, establish a unique and effective disaggregation and refolding
93 system. Interestingly, in the presence of ClpP, the successfully refolded substrate protein was
94 released and not transferred for ClpP degradation.

95 ## Results

96 **McsB is the main adaptor protein for the removal of subcellular protein aggregates by**
97 **ClpC**

98 To identify which of the adaptor proteins is responsible for the general role of ClpC in protein
99 homeostasis *in vivo*, we constructed a triple adaptor mutant strain (TAM) lacking the genes for
100 the three known ClpC adaptor proteins (Δ*mecA*Δ*ypbH*Δ*mcsB*). This TAM strain was impaired
101 in thermoresistance and in its ability to develop thermotolerance (Fig 1A & S1A) (Runde et al.,
102 2014). To examine the individual impact of the different adaptor proteins, we re-introduced
103 each of the deleted genes under the control of the IPTG-inducible *hyper spank* (hs) promoter
104 (P_{hs}) in the *amyE* locus, allowing the independent expression of each adaptor protein in the
105 TAM strain (Fig 1BC Fig S1BD). We observed that only the expression of *mcsB*, and not *ypbH*

or *mecA*, was able to confer thermoresistance and thermotolerance at a level comparable to the wildtype strain of *B. subtilis* (Fig 1B, Fig S1BC). Only the expression of *mcsB* resulted in the complete removal of heat-induced protein aggregates after a 90 min recovery at 37 °C (Fig 1C, FigS1E) (Hantke et al., 2019). Furthermore, McsB-GFP co-localizes with subcellular protein aggregates marked by the YocM-mCherry reporter *in vivo* (Fig S1FG) (Kirstein et al., 2008). These experiments suggest that McsB is the ClpC adaptor protein necessary and sufficient for thermoresistance and thermotolerance development and to target subcellular protein aggregates for ClpC dependent removal (Hantke et al., 2019) (Fig 1 & Fig S1).

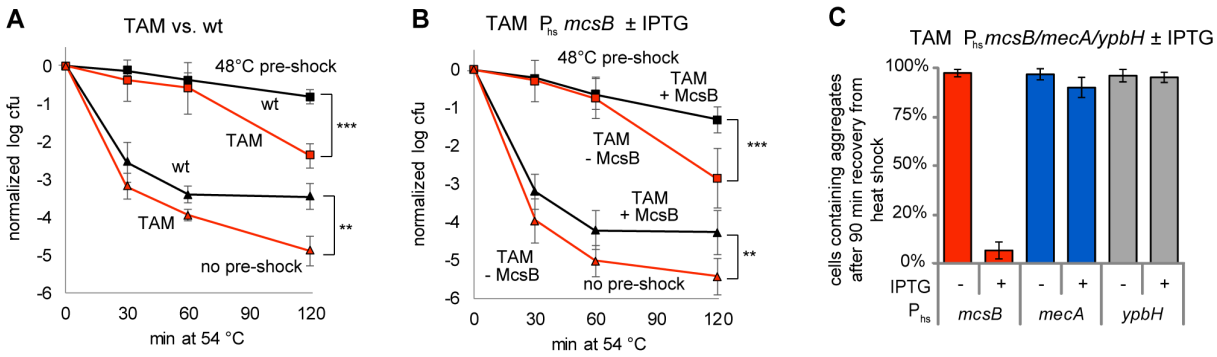

Figure 1 Role of ClpC adaptor protein McsB in protein homeostasis

A) Thermotolerance (squares: with pre-shock) and Thermoresistance (triangles: without pre-shock) experiments analyzing *B. subtilis* Δ*mecA*Δ*ypbH*Δ*mcsB* ('TAM', BIH737, red) and wildtype (black) strains. **B**) *B. subtilis* TAM P_{hs} *mcsB* strain (BIH739), with (black) and without IPTG (red) were examined in a thermotolerance (squares: with pre-shock at 48 °C) and thermoresistance (triangles: no pre-shock) experiment. Log_{10}-values of viable cell count were normalized, and three biological replicates were used to calculate standard deviations (error bars) with significant differences indicated (*: $p<0.05$, **: $p<0.01$, ***: $p<0.001$). **C**) Subcellular protein aggregates during recovery after heat stress *in vivo*. Ratio of cells containing protein aggregates marked by YocM-mCherry of complemented *B. subtilis* TAM strains (TAM P_{hs} *mscsB* (BIH739), TAM P_{hs} *mecA* (BIH740), TAM P_{hs} *ypbH* (BIH741), which were heat shocked for 30 min at 50°C and recovered for 90 min at 37°C, was determined based on three biological replicates including three technical replicates of 50 – 100 cells. Samples were taken at indicated time points for analysis by fluorescence microscopy (see also Fig S1D).

We used heat-aggregated and inactivated malate dehydrogenase (Mdh) as a model substrate for measuring the disaggregation and refolding activities of this chaperone system *in vitro* (Goloubinoff et al., 1999; Haslberger et al., 2008; Schlothauer et al., 2003). In a control experiment, we confirmed that the native, enzymatically active, and folded Mdh was not inactivated by the McsB kinase (Fig S1J).

134 We observed a fast disaggregation kinetic for the *E. coli* ClpB, DnaK, DnaJ and GrpE
135 disaggregation and refolding system, fully dissolving the protein aggregates and recovering
136 30% of enzyme activity after 120 minutes of incubation (Fig S1H). A slower disaggregation to
137 about 50% with a less effective refolding activity to about 15% of the initial Mdh activity could
138 be observed for the MecA/ClpC chaperone system (Schlothauer et al., 2003) (Fig S1H).
139 Adding McsB, McsA & ClpC to the heat-aggregated Mdh first increased light scattering,
140 peaking after 15 min, possibly indicating an apparent initial complex formation. The subsequent
141 disaggregation of the substrate protein reached only a level of 60% disaggregated protein
142 compared to 100% observed for ClpB/KJE (Fig S1H, left panel). Only very little refolding
143 (about 5%) could be observed for McsB and McsA with ClpC (Fig S1H, right panel).
144 In supernatant/pellet experiments, only the solubilization of aggregated Mdh by ClpB/KJE
145 could be detected (Fig S1I). With an antibody generated to detect protein arginine
146 phosphorylation (Fuhrmann et al., 2015), we observed that most of the phosphorylated substrate
147 could be detected after 15 min, mostly in the soluble fraction (Fig S1I). This coincides with the
148 initial disaggregation complex appeared to become stabilized and active (Fig S1H, Fig S1I).
149 The significant disaggregation but rather low refolding activity by ClpC, McsB and McsA (Fig
150 S1H) might be explained by the unhinged kinase activity of McsB (Fig S1I), whereby the
151 protein arginine phosphorylation of the substrate protein could interfere with its successful
152 refolding.

153 **McsB lacking its kinase activity can partially function as a ClpC adaptor protein in**
154 **protein disaggregation and refolding**

155 Therefore, we investigated the kinase-inactive McsB C167S variant (Kirstein et al., 2005, 2007)
156 in these *in vivo* and *in vitro* experiments. A *mcsB* deletion mutant and the kinase-inactive
157 *mcsB* C167S mutant strain were impaired by about one order of magnitude in their ability to
158 develop thermotolerance or thermoresistance (Fig S2A). However, a partial disaggregation
159 activity at about 25% of the wt *B. subtilis* level was still observed *in vivo* for the *mcsB* C167S

160 mutant, while no *in vivo* disaggregation activity was detected during recovery at 37°C in the
161 absence of McsB or McsB C167S (Fig S2B). McsB C167S could still activate the ClpC ATPase
162 activity *in vitro*; however, only to less than 50 % of McsB-mediated activation (Fig S2C). We
163 could observe a similar *in vivo* co-localization to subcellular protein aggregates by the kinase-
164 inactive McsB C167S-GFP and the McsB-GFP fusion proteins (Kirstein et al., 2008),
165 suggesting that McsB can recognize subcellular protein aggregates independently of its kinase
166 activity (Fig S2D).
167 McsB C167S was able to facilitate the ClpC mediated disaggregation reaction *in vitro*, albeit
168 not as fast as wt McsB with McsA, but reaching a similar yield after 120 min (Fig S2E).
169 However, with McsB C167S, we observed a significantly increased recovery of Mdh activity
170 by about 20% of the initial activity compared to the 5% of wt McsB with McsA (Fig. S2E) or
171 the 15% of MecA (Fig S1H). This suggests that the McsB C167S variant could still bind and
172 activate ClpC and concurrently recognize and target aggregated proteins to a certain extent of
173 disaggregation and refolding, even in the absence of arginine phosphorylation (Fig S2E & S2F).
174 **The presence of sub-stoichiometric amounts of the YwlE phosphatase is necessary to**
175 **facilitate McsB kinase-mediated *in vitro* disaggregation and refolding by ClpC**
176 McsA-activated McsB appeared to facilitate disaggregation but, in contrast to the kinase-
177 inactive McsB C167S variant, very little refolding of aggregated Mdh was observed (Fig S2E
178 & S2F). This suggests that controlling the level of protein arginine phosphorylation state by the
179 missing cognate phosphatase YwlE could be important for this chaperone system (Elsholz et
180 al., 2012; Schmidt et al., 2014). Previous *in vitro* experiments demonstrated that equimolar
181 amounts of YwlE inhibit the McsB and McsA-mediated activation of ClpC (Kirstein et al.,
182 2007). Therefore, we tested the effect of lowering the YwlE concentration on the ClpC ATPase
183 activity and observed that at sub-stoichiometric amounts of 0.01-0.05 µM of YwlE, the McsA
184 & McsB induced ClpC ATPase activity was not inhibited anymore (Fig 2A).

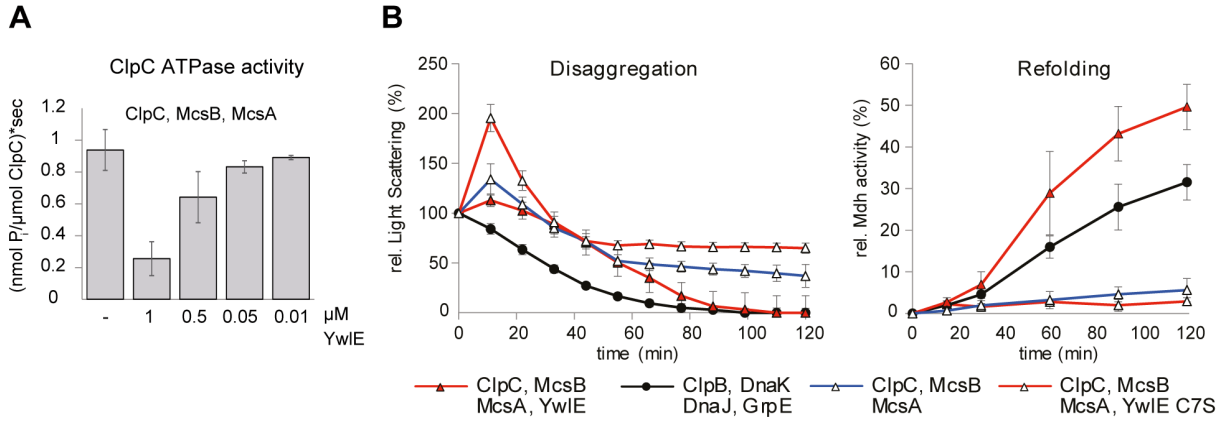

Figure 2 Sub-stoichiometric YwlE facilitates *in vitro* disaggregation and refolding

A) ATPase activity of ClpC/McsB/McsA (1/1/1 µM) was determined in absence or presence of indicated amounts of YwlE (0.01-1µM). **B**) Disaggregation and refolding experiments. Disaggregation of heat aggregated Mdh after addition of ClpB/KJE (filled black circles), ClpC/McsB/McsA (empty triangles, blue line), ClpC/McsB/McsA/YwlE (red filled triangles) or ClpC/McsB/McsA/YwlE C7S (empty triangles, red line) was monitored *in vitro* by measuring light scattering at 30 °C for 120 min (left panel). The refolding was determined by Mdh enzymatic activity (right panel). 0.05 µM YwlE or YwlE C7S were added when indicated. The plots show the mean of at least three replicates with standard deviation.

When we added such a sub-stoichiometric amount of YwlE (0.05 µM) to the *in vitro* disaggregation and refolding assay with ClpC, McsB & McsA (at 1.5, 1 & 1 µM), we observed an enhanced disaggregation of aggregated Mdh and a significantly increased refolding (Fig 2B). Remarkably, about 100% of the heat-aggregated Mdh was disaggregated before 90 min, and 50% was successfully refolded by ClpC, McsB & McsA in the presence of the low amount of YwlE. Accordingly, pellet-supernatant experiments displayed a clear shift of Mdh from the pellet to the soluble fraction in the presence of ClpC, McsB & McsA with sub-stoichiometric amounts of YwlE. Interestingly, arginine protein phosphorylation was close to or even below detection level by western blot (Fig S3A), suggesting that the presence of sub-stoichiometric amounts of active YwlE is sufficient to effectively lower the phosphorylation state of the involved proteins.

When we added the same sub-stoichiometric amount of the phosphatase inactive YwlE C7S variant (Fuhrmann et al., 2013) to the disaggregation and refolding experiment, we observed a more pronounced shift in light scattering, suggesting a larger protein complex formation after 15 min accompanied by a low disaggregation rate without apparent refolding (Fig 2B).

210 Furthermore, no solubilization of aggregated protein could be observed in the respective
211 supernatant pellet experiment with YwlE C7S (Fig S3A). In the presence of the YwlE C7S
212 variant, the concomitant protein arginine phosphorylation was at a maximum after 15 min,
213 concurrent with the raised light scattering signal observed in the absence of YwlE (Fig 2B &
214 S3A). With order-of-addition experiments, we observed that the later the addition of YwlE was,
215 the lower the disaggregation and the refolding yields were (Fig S4AB).
216 These experiments suggest that the YwlE phosphatase activity is necessary for efficient
217 disaggregation and refolding by the ClpC/McsB/McsA chaperone system. YwlE-mediated de-
218 phosphorylation might directly support refolding of unfolded substrate proteins (Fig 2B) and
219 could also modulate ClpC, McsB and McsA activities (Elsholz et al., 2012; Hajdusits et al.,
220 2021; Kirstein et al., 2007; Schmidt et al., 2014).

221 **Low *in vivo* levels of the YwlE phosphatase are necessary for protein homeostasis**

222 Our *in vitro* experiments suggested that the presence of sub-stoichiometric levels of YwlE
223 relative to the ClpC chaperone complex (1:20-1:30) facilitates efficient McsB-mediated
224 disaggregation and refolding of aggregated proteins. This ratio of YwlE to ClpC corresponds
225 relatively well to the observed *in vivo* ratio of about 20 to 100 times lower *in vivo* cellular
226 concentration of YwlE, compared to the higher abundant ClpC (Gerth et al., 2004; Muntel et
227 al., 2014; Turgay et al., 1998).
228 *B. subtilis* lacking *ywlE* was more thermosensitive and less thermotolerant than the wildtype
229 strain (Fig 3A), similar to what we observed for Δ*mcsB* cells (Fig S2A & S2E). Since the
230 relative levels of YwlE seem to play an important role, we wanted to assess the effect of
231 different cellular levels of YwlE on heat stress response and protein homeostasis in more detail.
232 Therefore, we complemented the Δ*ywlE* mutant *in trans* by IPTG inducible expression of *ywlE*
233 or *ywlE* C7S in the *amyE* locus.
234 We then estimated the cellular YwlE levels of these strains by quantitative western blotting (Fig
235 3D & S3E). We observed levels of about 134 (±34) and 64 (±11) YwlE molecules per cell in

236 in wildtype *B. subtilis* and the complemented Δ*ywlE* P_{hs} *ywlE* strain without IPTG addition,
237 respectively (Fig S3E). Already the addition of 10 µM IPTG doubled the cellular YwlE to 274
238 (± 26) molecules/cell, going up to about 6500 (± 1702) molecules YwlE per cell when 2 mM
239 IPTG was added (Fig 3D & S3E). We observed that without induction, the Δ*ywlE* P_{hs} *ywlE*
240 strain (about 64 molecules per cell) behaved like the wildtype (about 134 molecules per cell) in
241 protein homeostasis. The more IPTG inducer was added, the more YwlE was expressed, and
242 the less thermotolerant and thermoresistant these cells became (Fig 3AC & S3C), comparable
243 to the strains lacking YwlE or McsB (Fig S2A & 3AC). Thermotolerance and thermoresistance
244 were as low as in a Δ*ywlE* strain when complementing with the phosphatase inactive *ywlE* C7S
245 variant (Fig 3C).

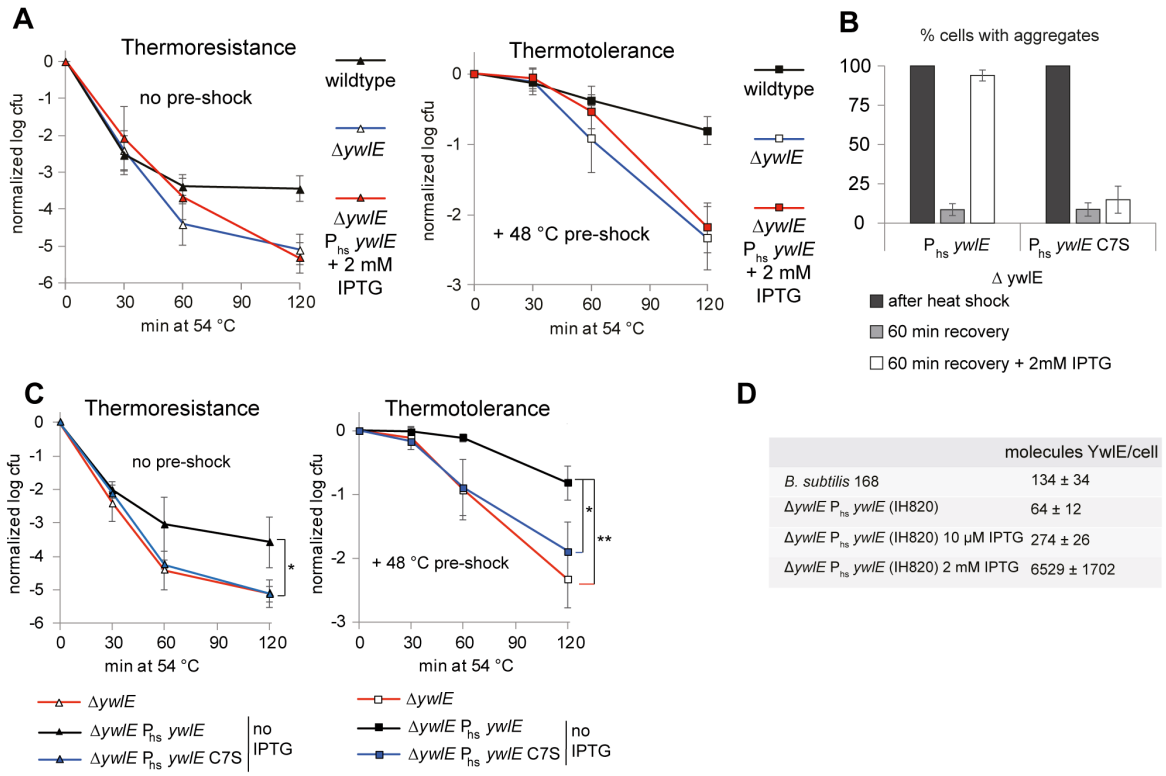

246
247 **Figure 3 Low *in vivo* levels of YwlE facilitate protein homeostasis**
248 **A**) Thermoresistance (left panel no pre-shock) and thermotolerance (right panel15 min pre-shock at 48 °C)
249 experiments with *B. subtilis* wildtype (black), Δ*ywlE* (BIH309, blue) and Δ*ywlE* P_{hs} *ywlE* + 2 mM IPTG
250 (BIH828, red) were performed. Log_{10}-values of viable cell counts were normalized and three biological
251 replicates were used to calculate standard deviations (error bars). **B**) Subcellular protein aggregates during
252 recovery after heat stress *in vivo*. Cells of *B. subtilis* strains Δ*ywlE* P_{hs} *ywlE* (BIH828) and Δ*ywlE* P_{hs} *ywlE*
253 C7S (BIH829) both also encoding P_{xyl} *yocM-mCherry* were heat shocked for 20 min at 52°C and recovered

for 60 min at 37°C. Cells were taken at the indicated timepoints and their subcellular protein aggregates analyzed by fluorescence microscopy. Three biological replicates including three technical replicates with about 50 – 100 cells were analyzed to calculate the ratio of cells containing protein aggregates marked by YocM-mCherry. **C**) Thermoresistance (left panel no pre-shock) and thermotolerance (right panel 15 min pre-shock at 48 °C) experiments with *B. subtilis* Δ*ywlE* (BIH309, red), Δ*ywlE* P_{hs} *ywlE* (BIH828, black) and Δ*ywlE* P_{hs} *ywlE* C7S (BIH829, blue) without IPTG. Log_{10}-values of viable cell count were normalized, and three biological replicates were used to calculate standard deviations (error bars) with significant of differences indicated (*: $p<0.05$, **: $p<0.01$, ***: $p<0.001$, Welch's test). **D**) Table showing the number of YwlE proteins / cell determined *in vivo* by quantitative Western blotting for the different *B. subtilis* strains and indicated IPTG concentrations (see Fig S3E).

Assessing the subcellular aggregate formation revealed increased subcellular aggregates at 48°C and at 48/53°C during thermotolerance for the cells with increased *ywlE* expression, but not when *ywlE* C7S was expressed (Fig S3B). In line with these experiments, high expression of *ywlE* diminished the clearance of heat-induced aggregates during recovery from heat stress (Fig 2D), which was not observed with low YwlE levels or for the Δ*ywlE* strain complemented with the highly expressed *ywlE* C7S (Fig 3B).

Interestingly, we did not observe an influence of *ywlE* expression on the level of subcellular aggregates during recovery from heat stress in a kinase-inactive *mcsB* C167S mutant (Fig S3D), confirming that the presence of protein arginine phosphorylation activity is required for the counteracting *ywlE* phosphatase mediated phenotypes to occur.

High levels of YwlE phosphatase interfere strongly with the McsB kinase and thereby impede its positive influence on ClpC-mediated protein homeostasis, both *in vitro* and *in vivo*. Controlling the cellular protein arginine phosphorylation state is therefore not only mediated by the McsA-activated McsB kinase but has to be limited by the YwlE phosphatase, which, at a certain sub-stoichiometric ratio to McsB, can counteract its kinase activity at a level which facilitates a well-functioning *B. subtilis* protein homeostasis.

The ClpC unfolding activity is not directly influencing the subsequent YwlE-dependent refolding of unfolded phosphorylated substrate protein *in vitro*

We wanted to assess whether the ClpC chaperone activity directly affects the YwlE-dependent refolding of already unfolded phosphorylated substrate proteins. We employed a ClpC trap

285 variant (ClpC-DWB), which by forming mixed complexes, inhibits the ClpC ATPase and
286 unfoldase activity (Fig S4C & S4D) (Babst et al., 1998; Kirstein et al., 2006; Weibezahn et al.,
287 2003; Ye et al., 2001).
288 The McsB, McsA & ClpC mediated disaggregation was initiated and ClpC-DWB was added
289 after 15 min when the larger protein complex formed and the maximal substrate protein arginine
290 phosphorylation was observed (Fig S4C, Fig 2B & Fig S3A). As expected, the addition of
291 ClpC-DWB led to the formation of a more extended binding peak and a halt of disaggregation,
292 resulting in a decline to a lower but constant light scattering signal for the remaining time (Fig
293 S4C), suggesting that the mixed ClpC/ClpC-DWB oligomers were not able to further process
294 the aggregated substrate proteins (Kirstein et al., 2006). Simultaneous or subsequent addition
295 of YwlE (at 15 (green squares) or 20 min (blue diamonds)), but not the addition of YwlE C7S
296 (at 15 min (purple circles)), appeared to disrupt the apparent complex formation leading to drop
297 to a similar lower level of constant light scattering, caused by ClpC-DWB addition (Fig S4C).
298 Nevertheless, the addition of active YwlE facilitated up to 15 % recovery of enzyme activity
299 after 120 min (green squares), despite ClpC-DWB inhibiting the disaggregation at that point.
300 No considerable refolding occurred when YwlE C7S variant was added (purple circles) (Fig
301 S4C). These experiments are consistent with the hypothesis that the YwlE phosphatase activity
302 could support the refolding of previously unfolded and phosphorylated substrate proteins even
303 while the ClpC activity was inhibited (Fig S4C).

304 **The activation of McsB by McsA is necessary to initiate the disaggregation and refolding**
305 **reaction *in vitro***

306 To investigate the McsB kinase activator McsA in more detail, we added McsA at different
307 timepoints to the reaction (Fig S4E). A constant stable light scattering signal was detected,
308 when no McsA was added to ClpC, McsB & YwlE incubated with aggregated Mdh. Adding
309 McsA immediately increased the light scattering signal suggesting an initial protein complex
310 formation, followed by the onset of the disaggregation reaction and Mdh activity starting to

311 become recovered. The refolding yield correlated to the length of disaggregation time after the
312 McsA addition (Fig S4E). Already about 5 min after McsA addition, the start of protein arginine
313 phosphorylation of ClpC, McsB and McsA could be detected, confirming the activation of the
314 McsB kinase activity by McsA (Fig S4F). These experiments suggest that McsB activation by
315 McsA is necessary to initiate the efficient disaggregation and subsequent refolding activity by
316 this chaperone system.

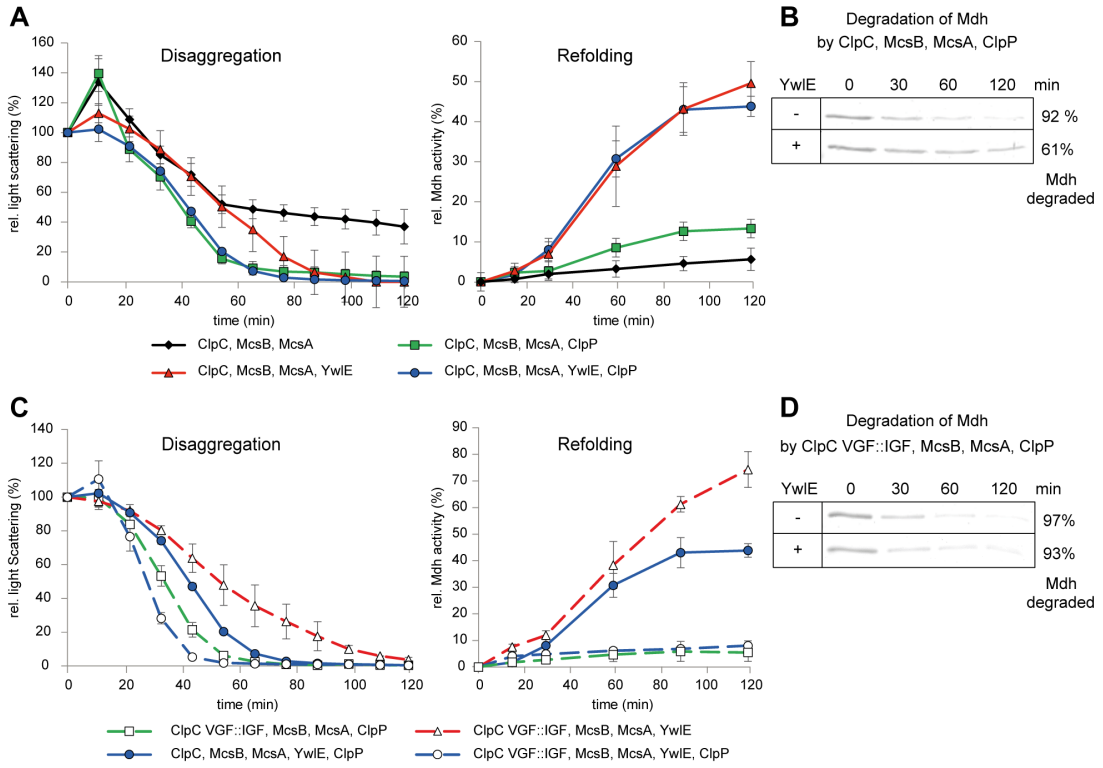

317

318 **Figure 4 Influence of YwlE on ClpCP protease complex activity**
319 Disaggregation, refolding and degradation experiments. **A**) Disaggregation of heat aggregated Mdh (1µM)
320 after addition of ClpC/ McsB/ McsA (empty diamonds, black) ClpC/ McsB/ McsA/ ClpP (filled diamonds,
321 black), ClpC/ McsB/ McsA/ YwlE (empty circles, red) and ClpC/ McsB/ McsA/ YwlE/ ClpP (filled circles,
322 red) was monitored *in vitro* by measuring light scattering at 30 °C for 120 min (left panel). The concurrent
323 refolding was examined by measuring the Mdh enzymatic activity at the indicated time points (right panel).
324 **B**) *In vitro* degradation experiments of heat aggregated Mdh as substrate were performed with ClpC/ McsB/
325 McsA/ ClpP in the presence or absence of YwlE. Samples for analysis by SDS PAGE and Coomassie stain
326 were taken after 0 min, 30 min, 60 min and 120 min. The relative amount of degraded Mdh after 120 min is
327 indicated. **C**) Disaggregation of heat aggregated Mdh (1µM) after addition of ClpC/ McsB/ McsA (filled
328 diamonds, black) ClpC VGF:IGF / McsB/ McsA (empty diamonds, black), ClpC/ McsB/ McsA/ YwlE (filled
329 squares, red), ClpC VGF:IGF / McsB/ McsA/ YwlE (empty squares, red) ClpC/ McsB/ McsA/ YwlE /ClpP
330 (filled triangles, blue) and ClpC VGF:IGF / McsB/ McsA/ YwlE (empty triangles, blue) was monitored *in*
331 *vitro* by measuring light scattering at 30 °C for 120 min (left panel). The concurrent refolding was examined
332 by measuring the Mdh enzymatic activity (right panel) **D**) *In vitro* degradation experiments of heat
333 aggregated Mdh as substrate were performed with ClpC VGF::IGF/McsB/McsA/ClpP in the presence or

334 absence of YwlE. Samples for analysis by SDS PAGE and Coomassie stain were taken after 0 min, 30 min,
335 60 min and 120 min. The relative amount of degraded Mdh after 120 min is indicated.
336

337 **ClpP association with ClpC: allowing a switch between repair or removal?**

338 Another important interacting partner of ClpC is the ClpP protease complex which associates
339 via the ClpC P-loops to form the ClpCP AAA+ protease complex (Amor et al., 2019; Kim et
340 al., 2001; Martin et al., 2007; Tryggvesson et al., 2012). Therefore, we investigated how the
341 presence of ClpP influences the *in vitro* disaggregation and refolding activity of McsB, McsA,
342 ClpC, with or without YwlE (Fig 4A&C).
343 Adding ClpP in the absence of YwlE significantly enhanced the disaggregation activity (Fig
344 4A, green squares) and about 90% of aggregated Mdh were degraded (Fig 4B). Still, about 10%
345 of the aggregated Mdh was refolded (Fig 4A, green squares). The raised disaggregation activity
346 (Fig 4A) is consistent with the observed concurrent induction of the ClpC ATPase activity by
347 adding the ClpP protease complex (Fig S5A). The additional presence of YwlE did not further
348 influence disaggregation efficiency, but resulted in about 40 % refolding of the aggregated Mdh
349 (Fig 4A, blue circles), similar to the reaction in the presence of YwlE but without ClpP (Fig
350 4A, red triangles). However, the remaining 60 % unfolded, not reactivated Mdh (Fig 4A, blue
351 circles) was targeted for degradation (Fig 4B).
352 This suggests a possible triage where the refolded Mdh species could escape the transfer to the
353 associated ClpP protease, but the still unfolded substrate proteins were successfully transferred
354 for degradation into the ClpP protease complex.
355 ClpC, unlike the disaggregase ClpB from *E. coli*, encodes a peptide loop to specifically interact
356 with apical binding pockets of the double-heptameric ClpP oligomer, allowing the formation
357 of a ClpCP protease complex (Kim et al., 2001; Kirstein et al., 2006; Weibezahn et al., 2004).
358 The P-loop of ClpC contains a VGF motif at its tip, while other Clp proteins like ClpX from *B.*
359 *subtilis* and *E. coli* or ClpA from *E. coli* possess IGF P-loops to facilitate this interaction.

360 Interestingly, it was demonstrated that in the context of *E. coli* ClpXP, the IGF loop allows a
361 tighter interaction between ClpX and ClpP compared to a VGF loop (Amor et al., 2019).
362 To analyze the likely difference between the VGF vs IGF P-loop for the interaction of ClpC
363 with ClpP, we utilized the information of the recently resolved Cryo-EM structure of a ClpX-
364 ClpP complex (Gatsogiannis et al., 2019). Here, the IGF P-loops in the binding pockets of the
365 ClpP complex are well resolved, which allows to use of this structural information, together
366 with the *B. subtilis* ClpP structure (Lee et al., 2010), as templates to model and calculate
367 thermodynamic parameters to estimate the relative binding energies of these interactions. While
368 not all six possible P-loop complexes with the *B. subtilis* ClpP binding pocket show stronger
369 binding with Ile, overall, the calculated binding energy is clearly stronger with the Val-to-Ile
370 exchange (Fig S5E). These *in silico* modeling and calculations suggest a stronger binding
371 interaction of the IGF P-loop with the ClpP binding pockets, compared to the VGF P-loop,
372 indicated by the larger differences in the negative ΔΔG binding energy values due to the missing
373 methyl group in Val (Fig S5E).
374 To investigate the possible role of the interaction strength of the P-loop, we replaced the VGF
375 motif in ClpC with the ClpX IGF loop. Notably, the ClpC VGF::IGF variant displayed a slightly
376 lower ATPase (Fig S5B) and lower disaggregation activity (Fig 4C), but a high refolding
377 activity of up to 80% in the presence of YwlE (Fig 4C). Addition of ClpP to the experiment
378 with ClpC VGF::IGF enhanced the disaggregation activity and switched the proteolytic activity
379 of this complex to a full degradation of Mdh, independent of the presence of YwlE (Fig 4, Fig
380 S5D).
381 The observed complete degradation of the substrate protein by the ClpC VGF::IGF/ClpP AAA+
382 protease complex (Fig 4D) is in contrast to the only partial degradation of the remaining
383 unfolded substrate protein (Fig 4B). This difference suggests that a closer and possibly tighter
384 interaction of ClpC VGF::IGF with ClpP might interfere with the escape of already folded
385 substrate protein from wild type ClpC-ClpP (Fig 4AB). Such a relatively transient, dynamic

ClpC-ClpP interaction during disaggregation and unfolding could allow the more unconstrained folding of the extruding nascent peptide chains from ClpC and should also allow better access by the YwlE phosphatase.

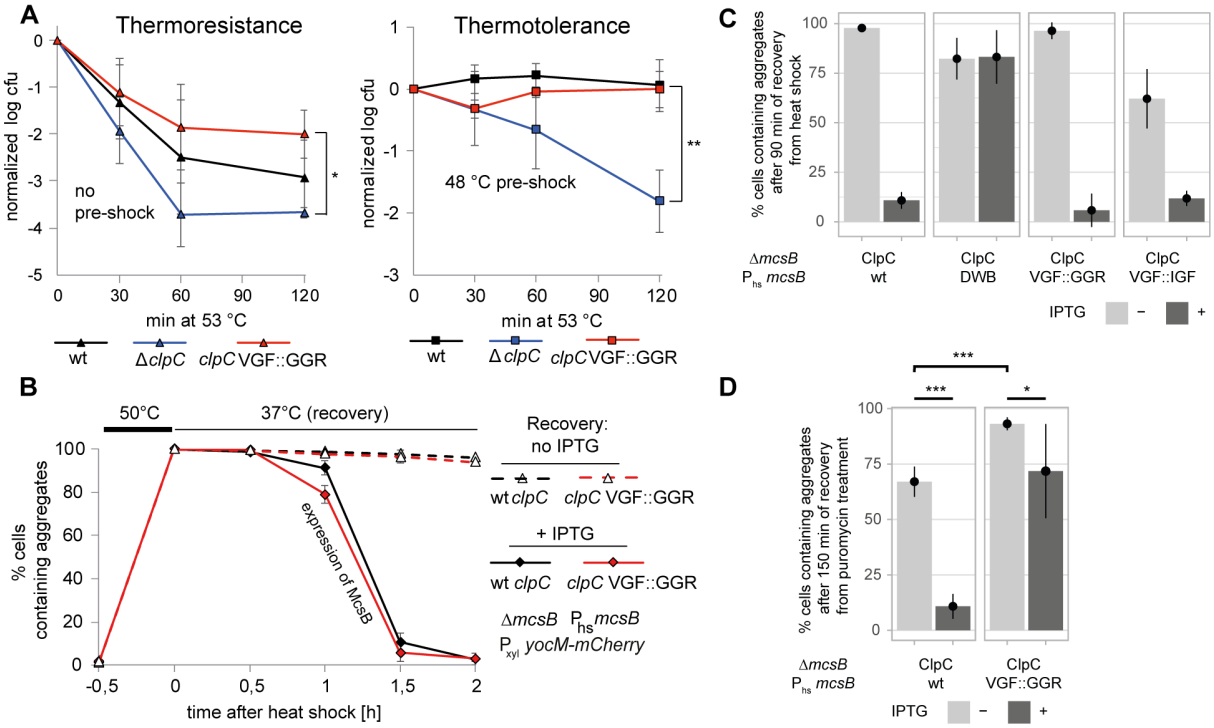

Figure 5 ClpC P-loop variants: rescue or removal?

A) Thermoresistance (left panel/triangles: no pre-shock) and thermotolerance (right panel/squares: 15 min pre-shock at 48 °C) experiments were performed with *B. subtilis* wildtype (black), Δ*clpC* (BIH19, blue) and *clpC* VGF::GGR (BIH217, red). Log_{10}-values of viable cell count were normalized and three biological replicates were used to calculate standard deviations (error bars) with significant differences indicated (*: p<0.05, **: p<0.01, ***: p<0.001, Welch's test). **B**) Cells of *B. subtilis* strains Δ*mcsB* P_{hs} *mcsB* P_{xyl} *yocM-mCherry* (BIH414, black), *clpC* VGF::GGR Δ*mcsB* P_{hs} *mcsB* P_{xyl} *yocM-mCherry* (BIH485, red) were treated 30 min with a 50 °C heat shock and subsequently shifted to recover for 120 min to 37 °C in the absence (triangles, dashed line), or presence of IPTG (diamonds). Samples were taken at indicated time points for fluorescence microscopy to calculate the ratio of cells containing protein aggregates marked by YocM-mCherry. **C**) ClpC wt (BIH414), ClpC-DWB (BIH488), ClpC VGF::GGR BIH485) and ClpC VGF::IGF (BIH860) strains (all with additional Δ*mcsB* P_{hs} *mcsB* P_{xyl} *yocM-mCherry*) were treated with a 50 °C heat shock and shifted for 90 min to 37 °C in the absence or presence of IPTG. Samples were taken at 90 min for fluorescence microscopy analysis to calculate the ratio of cells containing protein aggregates. Three biological replicates including three technical replicates with 50 – 100 cells were analyzed. Log_{10}-values of viable cell count were normalized and three biological replicates were used to calculate standard deviations (error bars). **D**) *B. subtilis* clpC wt (Δ*mcsB* P_{hs} *mcsB* P_{xyl} *yocM-mCherry* (BIH414)) and *clpC* VGF::GGR Δ*mcsB* P_{hs} *mcsB* P_{xyl} *yocM-mCherry* (BIH485)) were treated with 25 µg/mL puromycin. After 15 min, puromycin was removed and the cells incubated in fresh media with xylose in the presence or absence of 2 mM IPTG at 37 °C for 150 min. Samples were taken for analysis by fluorescence microscopy and western blot analysis with anti-McsB or anti-ClpC antibodies (see also S6F & G). The ratio of cells containing protein aggregates was determined based on three biological replicates including three technical replicates with 50 – 100 cells. Log_{10}-values of viable cell count were normalized and three biological replicates were used to

413 calculate standard deviations (shown as error bars) with significant differences indicated (*: $p<0.05$, **:
414 $p<0.01$, ***: $p<0.001$, Welch's test).
415
416 **A ClpC VGF::GGR variant, which cannot associate with ClpP, is functioning under heat**
417 **stress *in vivo*** Our *in vitro* results suggest that the ClpCP complex can switch between a
418 refolding and a degradation mode, depending on the interaction of its P-loop with ClpP (Fig 4).
419 To evaluate the ClpC function independent of ClpP *in vivo*, we constructed a *B. subtilis* mutant
420 strain, encoding a P-loop ClpC VGF::GGR variant, which abolishes the interaction with the
421 ClpP complex and has therefore no proteolytic activity neither *in vivo* nor *in vitro* (Fig S6AB)
422 (Kirstein et al., 2007; Turgay et al., 1998), but it is active in the *in vitro* disaggregation and
423 refolding experiment (Fig S6E), yet a slightly lower ATPase compared to ClpC is observed
424 (Fig S6D).
425 Interestingly, while a Δ*clpC* deletion mutant showed impaired thermotolerance development
426 and increased protein aggregation during heat shock *in vivo*, a *clpC* VGF::GGR and the *clpC*
427 VGF::IGF mutant strain behaved like the wildtype strain in thermotolerance (Fig 5A & Fig
428 S5C). The *clpC* VGF::GGR appeared to be a little more thermoresistant compared to wildtype
429 strain (Fig 5A). A Δ*clpC* strain forms more heat-induced aggregates *in vivo* than the wildtype
430 and the comparable *clpC* VGF::GGR mutant strain (Fig S6C).
431 In addition, McsB-mediated removal of heat-induced protein aggregates during recovery from
432 heat shock was not affected in a wildtype or a *clpC* VGF::GGR and the *clpC* VGF::IGF mutant
433 strain, but strongly impaired in the ATPase inactive *clpC* DWB background strain (Fig 5BC).
434 These results confirmed that the ClpC VGF::GGR variant, although not able to associate with
435 ClpP, could very well replace wt ClpC in response to the different heat stress conditions,
436 including thermotolerance, thermoresistance, and protein aggregate removal during recovery
437 from heat stress (Fig 5ABC, Fig S6C). To further test the ability of the ClpC VGF::GGR
438 variant, we applied a more severe proteotoxic stress induced by puromycin. Puromycin is
439 known to impair protein translation, generating toxic and persistent aggregates of misfolded,

440 incompletely synthesized protein fragments, which cannot be refolded. As expected, the
441 addition of puromycin led to the formation of protein aggregates (Fig 5D & Fig S6F). After
442 removing puromycin, we observed the clearance of protein aggregates in the *mcsB* deletion
443 mutant after 150 min, only when *mcsB* expression was induced (Fig 5D & Fig S6F). However,
444 clearance of the puromycin-generated truncated protein aggregates was diminished in the *clpC*
445 VGF::GGR mutant (Fig 5D & Fig S6F). This suggests that the ability to remove non-refoldable
446 protein aggregates by ClpCP mediated degradation can be beneficial under severe protein
447 folding stress.

448 **Discussion**

449 Here, we could identify the McsB kinase as the adaptor protein necessary and sufficient for
450 removing subcellular protein aggregates by ClpCP-mediated disaggregation through refolding
451 or degradation (Fig 1&2). In addition, we observed that a specific low sub-stoichiometric
452 amount of YwlE phosphatase was necessary to limit McsB kinase activities, allowing an
453 efficient modulation of ClpC-mediated disaggregation, unfolding and refolding (Fig2 & 3).
454 Consistent with this McsB kinase controlling the function of YwlE, we observed that both the
455 lack (Elsholz et al., 2012; Schmidt et al., 2014) and the excess of YwlE (Fig2, 3 & S3) resulted
456 in either unconstrained or inhibited McsB kinase activities, both negatively affecting the heat
457 shock response, ClpC function and protein homeostasis *in vivo* and *in vitro*.

458 The kinase activity of the McsB adaptor protein adds complexity but also expands the
459 recognition and targeting abilities of McsB. The activation of ClpC by McsB can be facilitated
460 by binding to the NTD of ClpC, but also by phosphorylation of specific arginine residues
461 located, for example, in the NTD of ClpC (Elsholz et al., 2012; Schmidt et al., 2014; Trentini
462 et al., 2016). We could observe some basal adaptor protein activity for the kinase-inactive McsB
463 C167S variant, and this activity is independent of YwlE (Fig S3). In contrast, the kinase-active
464 McsB only efficiently functions in the presence of a specific sub-stoichiometric level of the
465 YwlE phosphatase (Fig 2 & 3). Both activities can be complementary to one another since

466 McsB, like other adaptor proteins, can directly recognize and target substrate proteins to ClpC
467 even when these lack arginines (Elsholz et al., 2012; Kirstein et al., 2007; Stannek et al., 2014).
468 Importantly we observed that both McsB and McsB C167S could recognize sub-cellular protein
469 aggregates (Fig S2) and could subsequently help to recruit ClpC and ClpP (Kirstein et al., 2007,
470 2008), as also observed for DnaK acting as an adaptor protein for ClpB (Winkler et al., 2012).
471 A distinct substrate recognition and modification pathway by the McsB kinase was reported,
472 where McsB is not necessarily interacting directly with ClpC. Here these phospho-arginine
473 modifications of unfolded substrate proteins, generated by McsB, can act as a degron, which
474 allows the direct targeting and interaction of these marked substrate proteins via specific
475 phospho-arginine interaction sites in the NTD of ClpC (Morreale et al., 2022; Trentini et al.,
476 2016).
477 Interestingly, McsB, which forms a dimer, can further oligomerize upon heat shock to form an
478 octameric compartmentalized kinase, which allows the preferred access of unfolded protein
479 substrates for phosphorylation (Hajdusits et al., 2021; Suskiewicz et al., 2019). The activity and
480 formation of the McsB octamer and the ability of ClpC to directly recognize phospho-arginine
481 degron represent a possible additional path of substrates to be processed by ClpC. Unfolded
482 phosphorylated substrate proteins that exit ClpC and do not get dephosphorylated nor degraded
483 could then become directly retargeted by their still present degron to the binding site on the
484 NTD of ClpC (Trentini et al., 2016).
485 The arginine phosphorylation of unfolded, misfolded or aggregated protein species might
486 change the physical properties of these protein species in different ways. Arginine
487 phosphorylation switches a positive charge to the negative phosphoryl group, which can, for
488 example, interfere with the specific or unspecific interaction with DNA or RNA (Fuhrmann et
489 al., 2009). Protein aggregates formed from these differently charged misfolded phosphorylated
490 protein species might be physically better accessible. In addition, ClpC might interact directly

491 via its NTD with protein arginine phosphorylated misfolded proteins on the surface of such
492 protein aggregates (Trentini et al., 2016).
493 We observed that a specific cellular level of arginine phosphorylation is critical, and this level
494 can be controlled and limited by sub-stoichiometric amounts of YwlE, which was also essential
495 to allow the refolding of unfolded protein substrates of the McsA/McsB/ClpC chaperone system
496 (Fig 2 & 4). Here we hypothesize that the released unfolded and phosphorylated substrate
497 protein species might be unable to refold. However, in the presence of YwlE, the inhibiting
498 phosphoryl group can be removed, possibly allowing the refolding of the substrate protein.
499 Notably, a high-energy P-N bond is formed in phospho-arginine by McsB (Fuhrmann et al.,
500 2009; Teague and Dobson, 1999). This might be an important aspect when considering possible
501 thermodynamic energy requirements of the folding process accompanying the YwlE-mediated
502 protein arginine dephosphorylation.
503 Protein stability, folding and function are intricately connected to post-translational protein
504 modification (Beltrao et al., 2013; Mijakovic et al., 2016). It is well established that protein
505 modification by glycosylation and de-glycosylation play an important role in protein
506 homeostasis in the endoplasmic reticulum (Ellgaard and Helenius, 2003; Smith et al., 2011;
507 Walter and Ron, 2011). Interestingly, ubiquitination and de-ubiquitination by the cytosolic
508 deubiquitinating enzyme USP19 were observed to support membrane protein folding at the
509 cytosolic side of the ER membrane (Perrody et al., 2016). An interplay between unfolding and
510 protein de-modification was observed for the deubiquitinating enzyme Otu1, which interacts
511 with the C-terminus of AAA+ p97/CDC48 unfoldase and is important for releasing the
512 egressing ubiquitinated substrate protein during the endoplasmic reticulum-associated
513 degradation (Bodnar and Rapoport, 2017; Rumpf and Jentsch, 2006; Twomey et al., 2019).
514 In the presence of ClpC-associated ClpP, unfolded or misfolded substrate proteins are targeted
515 for ClpP degradation. However, already folded protein species are not transferred due to the
516 dynamic interaction of the P-loops with the ClpP oligomer (Fig 4). Such a relatively loose

517 ClpC-ClpP interaction would allow YwlE access to the egressing unfolded peptide from ClpC
518 to facilitate refolding by removing the possibly interfering arginine phosphate. This suggests
519 that the McsB/McsA/ClpCP/YwlE complex could switch between repair or degradation,
520 depending on the folding status of the substrate proteins.
521 The ability of a cellular protein homeostasis system to repair misfolded and aggregated proteins
522 can be advantageous since it allows the recovery of already synthesized proteins. Our *in vivo*
523 experiments demonstrated that a ClpC, not interacting with ClpP, was sufficient for well-
524 functioning cellular protein homeostasis even under heat stress conditions (Fig 5). This suggests
525 that the switch to the repair mode observed *in vitro* (Fig 4) can occur *in vivo* and might even be
526 prevalent (Fig 5). Nevertheless, the ability to form a functioning ClpCP protease complex
527 would allow removing toxic aggregates under severe stress (Fig 5) or controlling a transcription
528 factor's stability by regulatory proteolysis.

529 **Materials & Methods**

530 **General methods**

531 *B. subtilis* strains were grown in Lysogeny Broth medium (5 g l^{-1} yeast extract, 10 g l^{-1}
532 tryptone-peptone, 5 g l^{-1} NaCl) at 37 °C. Supplemental Table S1 shows the strains derived from
533 transformations of indicated plasmids or PCR products (Table S2) derived from cloning with
534 primers/restriction enzymes (Table S3) with standard cloning procedures (restriction enzymes
535 and T4 DNA ligase from NEB) as described previously (Sambrook and Russell, 2001). Cloning
536 was performed in *E. coli* DH5α (Invitrogen) (ampicillin 100 µg ml^{-1}, kanamycin 50 µg ml^{-1})
537 with Phusion High Fidelity Polymerase (NEB). Transformation into *B. subtilis* with
538 chromosomal or plasmid DNA was performed by standard methods (Anagnostopoulos and
539 Spizizen, 1961). Successful *amyE* insertion in *B. subtilis* was identified by assessing α-amylase
540 activity on plates with 0.4 % starch (w/v) and Lugol's iodine. Insertions in *amyE* and other
541 genomic sites such as *lacA* were confirmed by PCR.

542 **Protein purification**

543 Protein production was performed in *E. coli* BL21 (DE3) cells. Cells were grown at 37 °C to
544 an OD_{600} of 0.7 and induced with 1 mM IPTG overnight at 16 °C. Purification of His_6-tagged
545 proteins was performed by nickel affinity chromatography after cell lysis by French press.
546 YocM, McsB and McsB C167S were expressed and purified as N-terminal His-SUMO fusion
547 proteins, which were released by overnight cleavage with Ulp-protease at 4 °C (Andréasson et
548 al., 2008). ClpC, ClpC-DWB, ClpC-VGF:IGF, ClpC-VGF:GGR, ClpP, MecA, McsA, YwlE
549 and YwlEC7S were purified as previously described (Kirstein et al., 2005, 2006).

550 **Thermotolerance development and thermoresistance**

551 Thermotolerance development and thermoresistance experiments were performed as previously
552 described (Hantke et al., 2019; Runde et al., 2014). Cell cultures were separated at OD_{600} 0.4
553 and treated ± a 15 min pre-shock of 48°C before both samples were shifted to 53 °C or 54 °C.
554 Samples were taken for microscopy or plated on LB agar at t_0, t_{30}, t_{60} and $t_{120\ min}$. Obtained *cfu*
555 were plotted against time. At least three biological replicates were used to calculate standard
556 deviations, and statistical significance was calculated using Welch's test.

557 **Fluorescence microscopy**

558 *B. subtilis* cells were inoculated with a fresh overnight culture to an OD600 of 0.05 in LB +
559 0.5 % xylose (w/v) to express *yocM-mCherry* fusion (Hantke et al., 2019). Fluorescence
560 microscopy was performed at indicated time points on an object slide coated with 1 % agarose
561 (w/v) in saline (0.9 % NaCl (w/v)). Oil immersion and 10x100 magnifications were used with
562 a Zeiss fluorescence microscope with GFP and mCherry filters.

563 ***In vivo* disaggregation assay**

564 *B. subtilis* strains grown in LB + 0.5 % xylose (w/v) were treated at OD_{600} 0.25 – 0.3 with a
565 heat shock at 52 °C for 20 min or 50 °C for 30 mins if the strain lacks *mcsB*, which renders
566 them more sensitive towards heat stress (Fig 1C). Cultures were separated and ± 2 mM IPTG
567 was added while shifting the cells to 37 °C. Samples were taken for plating (colony forming

568 units (CFU)), western blotting and/or fluorescence microscopy as indicated. At least three
569 biological replicates were used to calculate standard deviations, and statistical significance was
570 calculated using Welch's test.

571 **Biochemical assays**

572 Light scattering and Mdh activity assays: Malate dehydrogenase (Roche) was inactivated and
573 aggregated by incubating 2 µM for 30 min at 47 C. Light scattering was determined at 360 nm
574 excitation and emission wavelength with a FP-6500-Spectrofluorometer (Jasco) at 30 °C.
575 1,5 µM ClpB, 1 µM DnaK, 0,2 µM DnaJ, 0,1 µM GrpE, 1,5 µM ClpC, 1 µM ClpP, 1 µM
576 MecA, 1 µM McsB, 1 µM McsA, 0,05 µM YwlE, proteins were incubated as indicated in the
577 respective experiments with 1 µM heat-treated Mdh in refolding buffer (50 mM Tris pH 7.8,
578 150 mM KCl, 20 mM $MgCl_2$, 2 mM DTT) supplemented with 20 µg/ml pyruvate kinase, 4 mM
579 phosphoenolpyruvate and 6 mM ATP as indicated in the respective experiments.

580 Mdh enzyme activity was determined before and after inactivation and at indicated time points
581 by diluting 2,5 µl reaction mixture in 125 µl Mdh activity buffer (150 mM potassium phosphate
582 buffer pH 7.6, 1 mM DTT, 0,5 mM oxalacetate, 0,28 mM NADH). The time dependent NADH
583 oxidation by Mdh was monitored at 340 nm in a Spectra Max MP3 Microplatereader
584 (Molecular Devices). At least three replicates of these experiments were analyzed, and the
585 resulting standard deviation included as error bars.

586 We also followed the protein aggregate solublization by supernatant pellet experiments.
587 Samples of the disaggregation and refolding experiments were taken at indicated time points,
588 centrifuged for 30 min, 14000 rpm at 4 °C. The supernatant was carefully separated from the
589 pellet, and mixed with the appropriate amount of 2xSDS sample buffer while the pellet, was
590 dissolved in 1 x SDS sample buffer to the same final volume. Both samples were incubated for
591 10 min at 90 °C and analyzed via SDS-PAGE and Coomassie stain (Schlothauer et al., 2003).
592 The in vitro degradation of aggregated Mdh or β-caseine in the presence of ClpP was analyzed
593 by SDS-PAGE and Coomassie stain. The relative amount of Coomassie stained protein band

594 was calculated using ImageJ analysis software to determine band intensities (Schneider et al.,
595 2012).
596 The ClpC ATPase activity was measured by phosphate release, colorimetrically detected with
597 the ammonium molybdate/malachite green assay as described previously (Lill et al., 1990;
598 Turgay et al., 1997). For this assay we used 1 µM ClpC, 1 µM ClpP, 1 µM MecA, 1 µM McsB,
599 1 µM McsA, 0,05 µM YwlE, and possible substrates such as 1 µM Mdh, 1 µM β-casein, as
600 indicated and if not mentioned otherwise. At least three replicates of the ATPase experiments
601 were implemented, and the resulting standard deviation was included as error bars.

602 **Western blotting**

603 SDS PAGE (15 % gels) loaded with similar amounts of protein (e.g. 5µg total protein for cell
604 extracts) was performed with standard methods as previously described (Laemmli 1970) with
605 anti-YwlE, anti-ClpC, anti-MecA, anti-McsB or anti-YpbH (Pineda Berlin) antiserum as
606 primary antibody and anti-rabbit alkaline phosphatase or horseradish peroxidase conjugate as
607 secondary antibody (1:10000). Blots were developed with standard BCIP (5 % (w/v) in DMF)
608 + 250 µL NBT (5 % (w/v) in 70 % DMF) or using the ECL western blotting reagent (GE
609 Healthcare).
610 For phospho arginine protein detection, samples were taken from light scattering assays,
611 without heat treatment prior to loading. SDS PAGE and western blotting on nitrocellulose were
612 performed at 4 °C. The primary anti-phosphoarginine-specific antibody was used 1:3000 with
613 5 % skim milk powder in TBS. Secondary antibodies and imaging was performed as described
614 above (Fuhrmann et al., 2015).

615 **YwlE quantification**

616 *B. subtilis* 168 (wild-type) and IH820 (Δ*ywlE*::*kanR* P_{lac} *ywlE* spec) cells were grown to an OD
617 0.35 ± 0.02. Subsequently, IPTG was added to a final concentration of 0.01 and 2 mM IPTG to
618 the IH820 cultures as indicated, which were further incubated for 30 min (Fig S3C). To
619 determine the number of bacteria, an aliquot was fixed with 3.7% formaldehyde in PBS and

620 cells were counted in a Petroff-Hauser chamber. Cell extracts were prepared by sonication and
621 western blotting was performed as mentioned above with few modifications. Samples were
622 resolved in 4-15% Mini-PROTEAN TGX precast gels and transferred to 0.22 µm PVDF
623 membranes. Anti-YwlE serum was used in a 1:5,000 dilution in 5% skim milk in TBS-T and
624 anti-rabbit IgG antibodies from goat conjugated to HRP were used 1:20,000 in the same buffer.
625 Blots were developed using a chemiluminescent substrate (Thermo Scientific, 34577) and
626 documented in a Fusion FX imaging system (Vilber). Defined amounts of purified YwlE-His
627 were included as a calibration curve on each gel (Fig S3C). The concentration of purified YwlE-
628 His was quantified by MS. Briefly, defined amounts of synthesized heavy isotope-coded YwlE
629 peptides (Table S4; JPT Peptide Technologies, Berlin) were spiked into a sample of the purified
630 YwlE protein. The concentration of the YwlE protein was then determined by dividing the MS
631 signal of the endogenous "light" peptides by the synthetic "heavy" peptides. Western blot
632 images were processed using Fiji (Schindelin et al., 2012).

633 **Structure modelling**

634 As a structural template for modelling the ClpC-ClpP interactions, we used the ClpP-ClpX
635 complex structure (PDB IDs: 6SFW, 6SFX) (Gatsogiannis et al., 2019). Each ClpX subunit and
636 the two interacting ClpP subunits were extracted and energy minimization was performed using
637 RosettaScripts (Fleishman et al., 2011) with the FastRelax (Khatib et al., 2011) mover and
638 strong coordinate constraints. To compare binding energies, the wt and ClpX I265V mutant
639 were again minimized, only allowing the backbone of the IGF-loop to move in an unconstrained
640 manner. Binding energies (ΔΔGbind) were calculated with the Rosetta energy function as
641 ΔGcomplex – (ΔGClpP,separated + ΔGClpC/X,separated) using the Rosetta InterfaceAnalyzer
642 application, allowing side chains to re-pack in the separated interactions partners. To estimate
643 the difference in binding in the *B. subtilis* ClpC-VGF and ClpC-IGF, the *B. subtilis* ClpP
644 structure representing the open conformation (PDB ID: 3KTK) (Lee et al., 2010) was
645 structurally aligned to 6SFX to have the L.m. ClpX IGF loops placed onto ClpP analogous to

646 the *L. monocytogenes* ClpP-ClpX complex structure. Due to the symmetry mismatch between
647 ClpP and ClpX, the six IGF loops were bound in distinct conformations, five of which are
648 relatively similar (conformation 1), whereas one loop has a different conformation
649 (conformation 2) (Fig S5E). In all conformations, changing Ile to Val diminishes the calculated
650 binding energy due to the missing methyl group in Val. (Fig S5E). Energy minimization and
651 binding energy calculations were done as described above.

652

653 **Author contributions** RA, IH, NM, EC & KT were involved in conceptualization. RA, IH,
654 FAC, KG & NM designed and performed the experiments. SR performed the *in silico* analysis
655 for the binding energies. IH, RA, FAC & KT wrote the initial manuscript. All authors
656 contributed to the manuscript writing, experimental design and analyzed the data. EC & KT
657 supervised the study and were responsible for funding acquisition.

658 **Funding** Work in our Lab was supported by the Deutsche Forschungsgemeinschaft (Tu106/6,
659 Tu106/8 (SPP1879) to KT & Leibniz-Price to EC) the Max Planck Society (EC & KT) and a
660 PhD fellowship from the Hannover School for Biomolecular Drug Research (HSBDR) to IH.

661 **Acknowledgements** We want to thank Jakob Fuhrmann (Scripps Research Institute) & Paul
662 Thompson (University of Massachusetts Medical School) for samples of the anti-phospho-
663 arginine antibody. David Dubnau (PHRI, Newark, NJ) & Axel Mogk (ZMBH, Uni Heidelberg)
664 for strains and plasmids. Alex Elsholz (MPUSP, Berlin) for discussion. Christian Frese and
665 Florian Kondrot (MPUSP, Berlin) for the proteomic analysis.

666 **References**

667 Amor, A.J., Schmitz, K.R., Baker, T.A., and Sauer, R.T. (2019). Roles of the ClpX IGF loops in ClpP
668 association, dissociation, and protein degradation. Protein Sci. Publ. Protein Soc. *28*, 756–765.
669 https://doi.org/10.1002/pro.3590.

670 Anagnostopoulos, C., and Spizizen, J. (1961). REQUIREMENTS FOR TRANSFORMATION IN BACILLUS
671 SUBTILIS. J. Bacteriol. *81*, 741–746. .

672 Babst, M., Wendland, B., Estepa, E.J., and Emr, S.D. (1998). The Vps4p AAA ATPase regulates
673 membrane association of a Vps protein complex required for normal endosome function. EMBO J *17*,
674 2982–2993. .

675 Battesti, A., and Gottesman, S. (2013). Roles of adaptor proteins in regulation of bacterial proteolysis.
676 Curr. Opin. Microbiol. *16*, 140–147. https://doi.org/10.1016/j.mib.2013.01.002.

677 Beltrao, P., Bork, P., Krogan, N.J., and van Noort, V. (2013). Evolution and functional cross-talk of
678 protein post-translational modifications. Mol. Syst. Biol. *9*, 714.
679 https://doi.org/10.1002/msb.201304521.

680 Bodnar, N., and Rapoport, T. (2017). Toward an understanding of the Cdc48/p97 ATPase.
681 F1000Research *6*, 1318. https://doi.org/10.12688/f1000research.11683.1.

682 Derre, I., Rapoport, G., and Msadek, T. (1999). CtsR, a novel regulator of stress and heat shock
683 response, controls clp and molecular chaperone gene expression in Gram-positive bacteria. Mol.
684 Microbiol. *31*, 117–131. https://doi.org/10.1046/j.1365-2958.1999.01152.x.

685 Ellgaard, L., and Helenius, A. (2003). Quality control in the endoplasmic reticulum. Nat Rev Mol Cell
686 Biol *4*, 181–191. .

687 Elsholz, A.K.W., Michalik, S., Zühlke, D., Hecker, M., and Gerth, U. (2010). CtsR, the Gram-positive
688 master regulator of protein quality control, feels the heat. EMBO J. *29*, 3621–3629.
689 https://doi.org/10.1038/emboj.2010.228.

690 Elsholz, A.K.W., Hempel, K., Michalik, S., Gronau, K., Becher, D., Hecker, M., and Gerth, U. (2011).
691 Activity Control of the ClpC Adaptor McsB in Bacillus subtilis ▿. J. Bacteriol. *193*, 3887–3893.
692 https://doi.org/10.1128/JB.00079-11.

693 Elsholz, A.K.W., Turgay, K., Michalik, S., Hessling, B., Gronau, K., Oertel, D., Mäder, U., Bernhardt, J.,
694 Becher, D., Hecker, M., et al. (2012). Global impact of protein arginine phosphorylation on the
695 physiology of Bacillus subtilis. Proc. Natl. Acad. Sci. U. S. A. *109*, 7451–7456.
696 https://doi.org/10.1073/pnas.1117483109.

697 Fei, X., Bell, T.A., Jenni, S., Stinson, B.M., Baker, T.A., Harrison, S.C., and Sauer, R.T. (2020). Structures
698 of the ATP-fueled ClpXP proteolytic machine bound to protein substrate. ELife *9*.
699 https://doi.org/10.7554/eLife.52774.

700 Fleishman, S.J., Leaver-Fay, A., Corn, J.E., Strauch, E.-M., Khare, S.D., Koga, N., Ashworth, J., Murphy,
701 P., Richter, F., Lemmon, G., et al. (2011). RosettaScripts: A Scripting Language Interface to the
702 Rosetta Macromolecular Modeling Suite. PLOS ONE *6*, e20161.
703 https://doi.org/10.1371/journal.pone.0020161.

704 Fuhrmann, J., Schmidt, A., Spiess, S., Lehner, A., Turgay, K., Mechtler, K., Charpentier, E., and Clausen,
705 T. (2009). McsB is a protein arginine kinase that phosphorylates and inhibits the heat-shock regulator
706 CtsR. Science *324*, 1323–1327. https://doi.org/10.1126/science.1170088.

707 Fuhrmann, J., Mierzwa, B., Trentini, D.B., Spiess, S., Lehner, A., Charpentier, E., and Clausen, T.
708 (2013). Structural basis for recognizing phosphoarginine and evolving residue-specific protein
709 phosphatases in gram-positive bacteria. Cell Rep. *3*, 1832–1839.
710 https://doi.org/10.1016/j.celrep.2013.05.023.

711 Fuhrmann, J., Subramanian, V., and Thompson, P.R. (2015). Synthesis and Use of a Phosphonate
712 Amidine to Generate an Anti-Phosphoarginine-Specific Antibody. Angew. Chem. Int. Ed Engl. *54*,
713 14715–14718. https://doi.org/10.1002/anie.201506737.

714 Gatsogiannis, C., Balogh, D., Merino, F., Sieber, S., and Raunser, S. (2019). Cryo-EM structure of the
715 ClpXP protein degradation machinery. Nat. Struct. Mol. Biol. *26*, 946–954.
716 https://doi.org/10.1038/s41594-019-0304-0.

717 Gerth, U., Kirstein, J., Mostertz, J., Waldminghaus, T., Miethke, M., Kock, H., and Hecker, M. (2004).
718 Fine-tuning in regulation of Clp protein content in Bacillus subtilis. J. Bacteriol. *186*, 179–191. .

719 Goloubinoff, P., Mogk, A., Zvi, A.P., Tomoyasu, T., and Bukau, B. (1999). Sequential mechanism of
720 solubilization and refolding of stable protein aggregates by a bichaperone network. Proc Natl Acad
721 Sci U A *96*, 13732–13737. .

722 Hahn, J., Kramer, N., Briley, K., and Dubnau, D. (2009). McsA and B mediate the delocalization of
723 competence proteins from the cell poles of Bacillus subtilis. Mol Microbiol *72*, 202–215.
724 https://doi.org/10.1111/j.1365-2958.2009.06636.x.

725 Hajdusits, B., Suskiewicz, M.J., Hundt, N., Meinhart, A., Kurzbauer, R., Leodolter, J., Kukura, P., and
726 Clausen, T. (2021). McsB forms a gated kinase chamber to mark aberrant bacterial proteins for
727 degradation. ELife *10*, e63505. https://doi.org/10.7554/eLife.63505.

728 Hantke, I., Schäfer, H., Janczikowski, A., and Turgay, K. (2019). YocM a small heat shock protein can
729 protect Bacillus subtilis cells during salt stress. Mol. Microbiol. *111*, 423–440.
730 https://doi.org/10.1111/mmi.14164.

731 Hartl, F.U., Bracher, A., and Hayer-Hartl, M. (2011). Molecular chaperones in protein folding and
732 proteostasis. Nature *475*, 324–332. https://doi.org/10.1038/nature10317.

733 Haslberger, T., Zdanowicz, A., Brand, I., Kirstein, J., Turgay, K., Mogk, A., and Bukau, B. (2008). Protein
734 disaggregation by the AAA+ chaperone ClpB involves partial threading of looped polypeptide
735 segments. Nat Struct Mol Biol *15*, 641–650. .

736 Khatib, F., Cooper, S., Tyka, M.D., Xu, K., Makedon, I., Popović, Z., Baker, D., and Players, F. (2011).
737 Algorithm discovery by protein folding game players. Proc. Natl. Acad. Sci.
738 https://doi.org/10.1073/pnas.1115898108.

739 Kim, Y.I., Levchenko, I., Fraczkowska, K., Woodruff, R.V., Sauer, R.T., and Baker, T.A. (2001).
740 Molecular determinants of complex formation between Clp/Hsp100 ATPases and the ClpP peptidase.
741 Nat Struct Biol *8*, 230-233. .

742 Kirstein, J., Zuhlke, D., Gerth, U., Turgay, K., and Hecker, M. (2005). A tyrosine kinase and its activator
743 control the activity of the CtsR heat shock repressor in B. subtilis. EMBO J *24*, 3435–3445. .

744 Kirstein, J., Schlothauer, T., Dougan, D.A., Lilie, H., Tischendorf, G., Mogk, A., Bukau, B., and Turgay, K.
745 (2006). Adaptor protein controlled oligomerization activates the AAA+ protein ClpC. EMBO J. *25*,
746 1481–1491. https://doi.org/10.1038/sj.emboj.7601042.

747 Kirstein, J., Dougan, D.A., Gerth, U., Hecker, M., and Turgay, K. (2007). The tyrosine kinase McsB is a
748 regulated adaptor protein for ClpCP. EMBO J. *26*, 2061–2070.
749 https://doi.org/10.1038/sj.emboj.7601655.

750 Kirstein, J., Strahl, H., Moliere, N., Hamoen, L.W., and Turgay, K. (2008). Localization of general and
751 regulatory proteolysis in Bacillus subtilis cells. Mol Microbiol *70*, 682–694.
752 https://doi.org/10.1111/j.1365-2958.2008.06438.x.

753 Kirstein, J., Molière, N., Dougan, D.A., and Turgay, K. (2009). Adapting the machine: adaptor proteins
754 for Hsp100/Clp and AAA+ proteases. Nat. Rev. Microbiol. *7*, 589–599.
755 https://doi.org/10.1038/nrmicro2185.

756 Krüger, E., and Hecker, M. (1998). The first gene of the Bacillus subtilis clpC operon, ctsR, encodes a
757 negative regulator of its own operon and other class III heat shock genes. J. Bacteriol. *180*, 6681–
758 6688. .

759 Krüger, E., Völker, U., and Hecker, M. (1994). Stress induction of clpC in Bacillus subtilis and its
760 involvement in stress tolerance. J Bacteriol *176*, 3360–3367. .

761 Krüger, E., Witt, E., Ohlmeier, S., Hanschke, R., and Hecker, M. (2000). The clp proteases of Bacillus
762 subtilis are directly involved in degradation of misfolded proteins. J Bacteriol *182*, 3259–3265. .

763 Krüger, E., Zühlke, D., Witt, E., Ludwig, H., and Hecker, M. (2001). Clp-mediated proteolysis in Gram-
764 positive bacteria is autoregulated by the stability of a repressor. EMBO J. *20*, 852–863.
765 https://doi.org/10.1093/emboj/20.4.852.

766 Lee, B.G., Park, E.Y., Lee, K.E., Jeon, H., Sung, K.H., Paulsen, H., Rubsamen-Schaeff, H., Brotz-
767 Oesterhelt, H., and Song, H.K. (2010). Structures of ClpP in complex with acyldepsipeptide antibiotics
768 reveal its activation mechanism. Nat Struct Mol Biol *17*, 471–478.
769 https://doi.org/10.1038/nsmb.1787.

770 Lill, R., Dowhan, W., and Wickner, W. (1990). The ATPase activity of SecA is regulated by acidic
771 phospholipids, SecY, and the Leader and mature domains of precursor proteins. Cell *60*, 271–280. .

772 Martin, A., Baker, T.A., and Sauer, R.T. (2007). Distinct static and dynamic interactions control
773 ATPase-peptidase communication in a AAA+ protease. Mol Cell *27*, 41–52. .

774 Mijakovic, I., Grangeasse, C., and Turgay, K. (2016). Exploring the diversity of protein modifications:
775 special bacterial phosphorylation systems. FEMS Microbiol. Rev. *40*, 398–417.
776 https://doi.org/10.1093/femsre/fuw003.

777 Mogk, A., Huber, D., and Bukau, B. (2011). Integrating protein homeostasis strategies in prokaryotes.
778 Cold Spring Harb. Perspect. Biol. *3*. https://doi.org/10.1101/cshperspect.a004366.

779 Mogk, A., Bukau, B., and Kampinga, H.H. (2018). Cellular Handling of Protein Aggregates by
780 Disaggregation Machines. Mol. Cell *69*, 214–226. https://doi.org/10.1016/j.molcel.2018.01.004.

781 Morreale, F.E., Kleine, S., Leodolter, J., Junker, S., Hoi, D.M., Ovchinnikov, S., Okun, A., Kley, J.,
782 Kurzbauer, R., Junk, L., et al. (2022). BacPROTACs mediate targeted protein degradation in bacteria.
783 Cell *185*, 2338-2353.e18. https://doi.org/10.1016/j.cell.2022.05.009.

784 Msadek, T., Kunst, F., and Rapoport, G. (1994). MecB of Bacillus subtilis, a member of the ClpC
785 ATPase family, is a pleiotropic regulator controlling competence gene expression and growth at high
786 temperature. Proc Natl Acad Sci U A *91*, 5788–5792. .

787 Muntel, J., Fromion, V., Goelzer, A., Maaβ, S., Mäder, U., Büttner, K., Hecker, M., and Becher, D.
788 (2014). Comprehensive absolute quantification of the cytosolic proteome of Bacillus subtilis by data
789 independent, parallel fragmentation in liquid chromatography/mass spectrometry (LC/MS(E)). Mol.
790 Cell. Proteomics MCP *13*, 1008–1019. https://doi.org/10.1074/mcp.M113.032631.

791 Perrody, E., Abrami, L., Feldman, M., Kunz, B., Urbé, S., and van der Goot, F.G. (2016). Ubiquitin-
792 dependent folding of the Wnt signaling coreceptor LRP6. ELife *5*.
793 https://doi.org/10.7554/eLife.19083.

794 Persuh, M., Mandic-Mulec, I., and Dubnau, D. (2002). A MecA paralog, YpbH, binds ClpC, affecting
795 both competence and sporulation. J Bacteriol *184*, 2310-3. .

796 Ripstein, Z.A., Vahidi, S., Houry, W.A., Rubinstein, J.L., and Kay, L.E. (2020). A processive rotary
797 mechanism couples substrate unfolding and proteolysis in the ClpXP degradation machinery. ELife *9*.
798 https://doi.org/10.7554/eLife.52158.

799 Rumpf, S., and Jentsch, S. (2006). Functional division of substrate processing cofactors of the
800 ubiquitin-selective Cdc48 chaperone. Mol. Cell *21*, 261–269.
801 https://doi.org/10.1016/j.molcel.2005.12.014.

802 Runde, S., Molière, N., Heinz, A., Maisonneuve, E., Janczikowski, A., Elsholz, A.K.W., Gerth, U.,
803 Hecker, M., and Turgay, K. (2014). The role of thiol oxidative stress response in heat-induced protein
804 aggregate formation during thermotolerance in Bacillus subtilis. Mol. Microbiol. *91*, 1036–1052.
805 https://doi.org/10.1111/mmi.12521.

806 Sambrook, J., and Russell, D.W. (2001). Molecular cloning: a laboratory manual (Cold Spring Harbor,
807 N.Y: Cold Spring Harbor Laboratory Press).

808 Sauer, R.T., and Baker, T.A. (2011). AAA+ proteases: ATP-fueled machines of protein destruction.
809 Annu. Rev. Biochem. *80*, 587–612. https://doi.org/10.1146/annurev-biochem-060408-172623.

810 Schindelin, J., Arganda-Carreras, I., Frise, E., Kaynig, V., Longair, M., Pietzsch, T., Preibisch, S., Rueden,
811 C., Saalfeld, S., Schmid, B., et al. (2012). Fiji: an open-source platform for biological-image analysis.
812 Nat. Methods *9*, 676–682. https://doi.org/10.1038/nmeth.2019.

813 Schlothauer, T., Mogk, A., Dougan, D.A., Bukau, B., and Turgay, K. (2003). MecA, an adaptor protein
814 necessary for ClpC chaperone activity. Proc. Natl. Acad. Sci. U. S. A. *100*, 2306–2311.
815 https://doi.org/10.1073/pnas.0535717100.

816 Schmidt, A., Trentini, D.B., Spiess, S., Fuhrmann, J., Ammerer, G., Mechtler, K., and Clausen, T. (2014).
817 Quantitative phosphoproteomics reveals the role of protein arginine phosphorylation in the bacterial
818 stress response. Mol. Cell. Proteomics MCP *13*, 537–550.
819 https://doi.org/10.1074/mcp.M113.032292.

820 Schneider, C.A., Rasband, W.S., and Eliceiri, K.W. (2012). NIH Image to ImageJ: 25 years of image
821 analysis. Nat. Methods *9*, 671–675. https://doi.org/10.1038/nmeth.2089.

822 Smith, M.H., Ploegh, H.L., and Weissman, J.S. (2011). Road to ruin: targeting proteins for degradation
823 in the endoplasmic reticulum. Science *334*, 1086–1090. https://doi.org/10.1126/science.1209235.

824 Stannek, L., Gunka, K., Care, R.A., Gerth, U., and Commichau, F.M. (2014). Factors that mediate and
825 prevent degradation of the inactive and unstable GudB protein in Bacillus subtilis. Front. Microbiol. *5*,
826 758. https://doi.org/10.3389/fmicb.2014.00758.

827 Suskiewicz, M.J., Hajdusits, B., Beveridge, R., Heuck, A., Vu, L.D., Kurzbauer, R., Hauer, K., Thoeny, V.,
828 Rumpel, K., Mechtler, K., et al. (2019). Structure of McsB, a protein kinase for regulated arginine
829 phosphorylation. Nat. Chem. Biol. *15*, 510–518. https://doi.org/10.1038/s41589-019-0265-y.

830 Teague, W.E., and Dobson, G.P. (1999). Thermodynamics of the arginine kinase reaction. J. Biol.
831 Chem. *274*, 22459–22463. .

832 Trentini, D.B., Suskiewicz, M.J., Heuck, A., Kurzbauer, R., Deszcz, L., Mechtler, K., and Clausen, T.
833 (2016). Arginine phosphorylation marks proteins for degradation by a Clp protease. Nature *539*, 48–
834 53. https://doi.org/10.1038/nature20122.

835 Tryggvesson, A., Ståhlberg, F.M., Mogk, A., Zeth, K., and Clarke, A.K. (2012). Interaction specificity
836 between the chaperone and proteolytic components of the cyanobacterial Clp protease. Biochem. J.
837 *446*, 311–320. https://doi.org/10.1042/BJ20120649.

838 Turgay, K., Hamoen, L.W., Venema, G., and Dubnau, D. (1997). Biochemical characterization of a
839 molecular switch involving the heat shock protein ClpC, which controls the activity of ComK, the
840 competence transcription factor of Bacillus subtilis. Genes Dev *11*, 119-28. .

841 Turgay, K., Hahn, J., Burghoorn, J., and Dubnau, D. (1998). Competence in Bacillus subtilis is
842 controlled by regulated proteolysis of a transcription factor. EMBO J. *17*, 6730–6738.
843 https://doi.org/10.1093/emboj/17.22.6730.

844 Twomey, E.C., Ji, Z., Wales, T.E., Bodnar, N.O., Ficarro, S.B., Marto, J.A., Engen, J.R., and Rapoport,
845 T.A. (2019). Substrate processing by the Cdc48 ATPase complex is initiated by ubiquitin unfolding.
846 Science *365*, eaax1033. https://doi.org/10.1126/science.aax1033.

847 Walter, P., and Ron, D. (2011). The unfolded protein response: from stress pathway to homeostatic
848 regulation. Science *334*, 1081–1086. https://doi.org/10.1126/science.1209038.

849 Weibezahn, J., Schlieker, C., Bukau, B., and Mogk, A. (2003). Characterization of a trap mutant of the
850 AAA+ chaperone ClpB. J Biol Chem *278*, 32608–32617.

851 Weibezahn, J., Tessarz, P., Schlieker, C., Zahn, R., Maglica, Z., Lee, S., Zentgraf, H., Weber-Ban, E.U.,
852 Dougan, D.A., Tsai, F.T.F., et al. (2004). Thermotolerance requires refolding of aggregated proteins by
853 substrate translocation through the central pore of ClpB. Cell *119*, 653–665.
854 https://doi.org/10.1016/j.cell.2004.11.027.

855 Winkler, J., Tyedmers, J., Bukau, B., and Mogk, A. (2012). Hsp70 targets Hsp100 chaperones to
856 substrates for protein disaggregation and prion fragmentation. J. Cell Biol. *198*, 387–404.
857 https://doi.org/10.1083/jcb.201201074.

858 Ye, Y., Meyer, H.H., and Rapoport, T.A. (2001). The AAA ATPase Cdc48/p97 and its partners transport
859 proteins from the ER into the cytosol. Nature *414*, 652–656. .

860 Zhou, B., Semanjski, M., Orlovetskie, N., Bhattacharya, S., Alon, S., Argaman, L., Jarrous, N., Zhang, Y.,
861 Macek, B., Sinai, L., et al. (2019). Arginine dephosphorylation propels spore germination in bacteria.
862 Proc. Natl. Acad. Sci. U. S. A. *116*, 14228–14237. https://doi.org/10.1073/pnas.1817742116.

863 Zhou, B., Alon, S., Rao, L., Sinai, L., and Ben-Yehuda, S. (2022). Reviving the view: evidence that
864 macromolecule synthesis fuels bacterial spore germination. MicroLife *3*, uqac004.
865 https://doi.org/10.1093/femsml/uqac004.

866